Article

A Basic Study on the Design of Dotted-Art Heterogeneous MPP Sound Absorbers

Kimihiro Sakagami *, Midori Kusaka and Takeshi Okuzono

Environmental Acoustics Laboratory, Department of Architecture, Graduate School of Engineering, Kobe University, Rokko, Nada, Kobe 657-8501, Japan; kusakamidori6@gmail.com (M.K.); okuzono@port.kobe-u.ac.jp (T.O.)
* Correspondence: saka@kobe-u.ac.jp

Abstract: Recently, dotted-art MPPs have been proposed in which a designed pattern is made with the holes. In such a case, the MPP becomes heterogeneous in general. However, existing theories used for the prediction of the absorption characteristics of MPPs assume homogeneity. Therefore, the elaboration of a method for heterogeneous MPPs needs to be performed. In previous work, the authors proposed a method to predict the absorption characteristics of a heterogeneous MPP by using synthesized impedances of each part with different parameters; this is called the synthetic impedance method (SIM) in the present paper. The SIM can potentially be used for various heterogeneous MPPs; however, its scope of applicability needs to be clarified. Furthermore, in proposing a design concept of dotted-art heterogeneous MPPs, the condition that would make the designed MPPs fall within the scope of the SIM needs to be determined. Therefore, in this study, in order to clarify the scope of the applicability of the SIM, twelve samples are first prepared, and then measured sound absorption characteristics and predicted ones are compared and examined in terms of prediction errors. The results show that there are two conditions that should be met to produce predictable heterogeneous MPPs: (1) holes are distributed over the entire surface of the specimen, and (2) the hole spacing is constant. Considering these conditions, a design concept for a dotted-art heterogeneous MPP is proposed: two types of holes, larger holes for the pattern and smaller holes for the background, should be used to meet the above two conditions. Case studies with nine prototypes show that the SIM can make predictions for dotted-art heterogeneous MPPs fabricated according to the concept described above.

Keywords: microperforated panel (MPP); heterogeneous MPP; dotted-art heterogeneous MPP; synthetic impedance method; sound absorption

1. Introduction

1.1. Background: Microperforated Panels (MPPs)

Since their proposal by Maa [1], microperforated panels (MPPs) have attracted wide attention as an alternative to porous sound-absorbing materials, and they are now established as one of the most promising sound-absorbing materials. MPPs are mainly composed of thin sheets or films with a thickness of 1 mm or less, and they are perforated with a diameter of 1 mm or less at a perforation ratio of approximately 1% or less. MPPs are basically composed of the same resonant sound-absorbing material as conventional perforated plates, but by using fine perforations, it can be said that they achieve the optimum acoustic impedance for sound-absorbing applications. Therefore, not only do MPPs achieve a higher absorptivity and a wider sound absorption bandwidth than conventional resonance-type sound absorbers, but they are also hygienic and durable and have excellent design properties unlike conventional porous sound-absorbing materials. The use of MPPs is expected to increase in the future as they are suitable for modern lifestyles [2].

MPPs have been extensively studied. In their early years, many researchers conducted studies on their applications and implementations for various purposes, including room

acoustics, plenum windows, and noise barriers [3–7]. However, the spread of these attractive sound-absorbing materials was limited because of the high-precision manufacturing technique and its cost. The MPPs produced in this period are called 'first-generation MPPs', which were mainly composed of metal sheets. Later, with advances in manufacturing techniques and the use of softer materials such as plastics and resin, their fabrication cost decreased. The MPPs produced in this period are called 'second-generation MPPs', and the spread and study of these materials were accelerated during this time [8,9]. This led to the recent growth of commercial products, which are aesthetically well-designed [10].

Most recently, Lee et al. [11] proposed artistically designed MPPs by using the dotted-art concept. In their paper, they introduced some examples of absorption materials which use the dotted-art concept with designs based on TV cartoon characters, among others. They also introduced ones with dotted-art designs that are commercially available. They showed that their prototypes had high sound absorptivity. They also compared their measured results with Maa's theory [1,12,13]; however, the prediction was not successful. The reason for this may be that their prototypes were not homogeneous, whereas Maa's theory assumes homogeneity. This also shows that artistically designed MPPs tend to be heterogeneous, and that their parameters are not uniformly distributed on the surface. In such a case, the existing prediction theory needs to be elaborated in order to extend it to heterogeneous cases. Lee et al. also showed an example of the prediction by synthesizing the impedances of the perforated part and the acoustically rigid part according to the method we proposed [14]; this point is discussed later.

However, other types of MPP absorbers with non-uniform parameters have been proposed by Sakagami et al. [15], Yairi et al. [16], and Mosa et al. [17]. In these works, MPP absorbers with different absorption characteristics are arranged in parallel to form a kind of array. As a result of this arrangement, all the absorption characteristics become broader and higher. These types of absorbers are often called 'inhomogeneous MPP absorbers', but in many cases, each absorber in the array is homogeneous, i.e., a combination of homogeneous MPP absorbers.

In the present paper, artistic MPPs designed using the dotted-art concept, which are usually heterogeneous, are studied. This type of MPP, of which the parameters are non-uniformly distributed on the entire surface of the material, is herein called 'heterogeneous' to distinguish it from 'inhomogeneous', as the latter is already widely known. In the next subsection, heterogeneous MPPs are discussed in detail.

1.2. Heterogeneous MPPs and Design-Oriented MPPs

As previously mentioned and discussed by Lee et al. [11], it is rather difficult to predict the absorption characteristics of dotted-art MPPs using the conventional method. Therefore, a prediction method for heterogeneous MPPs is needed in order to employ dotted-art MPPs in reality.

In cases where the heterogeneity is small, making predictions using the theory for homogeneous MPPs is somewhat possible. An example of this was given by Pan and Martellotta [18]. They studied a transparent MPP, but due to low manufacturing precision, the parameters were not uniform. They then used the average value of the hole diameter and were able to obtain a reasonable prediction.

An example of large heterogeneity was presented by Sakagami et al. [19]; in the same paper, MPPs fabricated using a 3D printer with low manufacturing precision were studied experimentally. The parameters, i.e., hole size and perforation ratio, were randomly distributed over the surface of each specimen, and although they showed rather high sound absorptivity, the theoretical prediction of the absorption coefficient was not successful. This failure was considered to have been caused by the heterogeneity of the samples.

Carbajo et al. [20] studied the acoustical properties of a heterogeneous perforated panel using the admittance sum method (ASM), parallel transfer matrix method (PTMM), equivalent circuit method (ECM), and finite element method (FEM) with the JCA model, and then compared the results [14]. They did not present the experimental results, but

they reported that all these analytical and numerical methods provided similar results. In addition, Carbajo et al. remarked that special attention must be paid to the type of back cavity configuration.

The current authors [14] previously presented a basic study on heterogeneous MPPs, on the surface of which the hole diameter and perforation ratio were heterogeneously distributed. In the same paper, a method for the prediction of sound absorption characteristics was proposed. Although the MPPs studied were heterogeneous, they consisted of locally homogeneous parts when closely inspected. Therefore, by synthesizing the impedances of these locally homogeneous parts, the total acoustic impedance was obtained with a method similar to the admittance sum method. We call this method the synthetic impedance method (SIM) in the present paper. The SIM gives reasonably good predictions. A summary of this method is provided in Section 2.

Regarding dotted-art MPPs, they are, in many cases, inevitably heterogeneous. As Lee et al. [11] discussed, Maa's theory does not give a good prediction. However, the absorption characteristics need to be predictable because the properties must be predicted in the design stage before they are actually used. As previously mentioned, Lee et al. [11] also examined the SIM [14] for one of their prototypes. According to their example, the SIM gave a reasonable prediction of the peak absorption coefficient and some errors in peak frequency, but the prediction was better than that based on Maa's theory [1,12,13]. They considered that the error was caused by the poor manufacturing accuracy of the prototype as well as by the approximation in the area of the perforated part used in the calculation.

Thus, it is important that the absorption characteristics of dotted-art MPPs are predicted in the design stage. In order to do this, either (1) a prediction method needs to be established or (2) a design method for an MPP that enables the prediction needs to be established. Considering the complexity of dotted-art MPPs, a general method that can make predictions for all types of artistic MPPs does not seem to be realistic. Therefore, as a practical solution, a design method that can produce dotted-art MPPs for which predictions can be made using an existing method needs to be established. For this purpose, the applicability of the existing method of prediction, the SIM [20], needs to be explored.

1.3. Outline of the Present Work

Considering the discussion above, this work is organized as follows: First, the prediction method that the authors previously proposed, the synthetic impedance method (SIM) [14], is introduced and examined experimentally to clarify its scope of application. Twelve samples of heterogeneous MPPs are measured, and the results are compared with the value predicted by the SIM (Sections 2 and 3). In this examination, we define three error indices, and predictability is explored in terms of prediction errors. As a result of this exploration, it is possible to obtain the design concept of a dotted-art heterogeneous MPP that enables the MPP to stay within the scope of the application so that its absorption characteristics can be predicted.

After determining the design concept of a dotted-art heterogeneous MPP, case studies with prototypes are conducted (Section 4): their normal absorption coefficients are measured and predicted for comparison. In the case studies, the abovementioned error indices are again used to explore prediction accuracy in terms of prediction errors.

Through the results, it is shown how a dotted-art heterogeneous MPP, whose sound absorption properties are predictable, can be made.

2. Prediction Method for the Absorption Characteristics of Heterogeneous MPPs

This section outlines the method used to predict the acoustic impedance of heterogeneous MPPs, which the authors proposed in a previous paper [14]. The specimens that are studied in the present paper are heterogeneous on the whole; however, in many cases, they are locally homogeneous in each part. Therefore, it is possible to consider that each sample consists of hypothetical MPPs in which holes of different diameters are arranged in a homogeneous way.

Suppose there is a specimen of surface area S, with holes of different diameters d_1, d_2, $\ldots$, d_n, and that its surface impedance is defined as Z_{MPP}. Then, it is assumed that for each hypothetical MPP with holes of specific diameters only in surface area S, the impedance is defined as $Z_{MPP,1}$, $Z_{MPP,2}$, $\ldots$, $Z_{MPP,n}$; that is, the impedance of a hypothetical MPP with a hole of diameter d_1 is $Z_{MPP,1}$, and the impedance of that with a hole of diameter d_2 is $Z_{MPP,2}$, etc. (see Figure 1). In this study, Guo's theory [21–24] (see Appendix A) is employed to calculate $Z_{MPP,1}$, $Z_{MPP,2}$, $\ldots$.
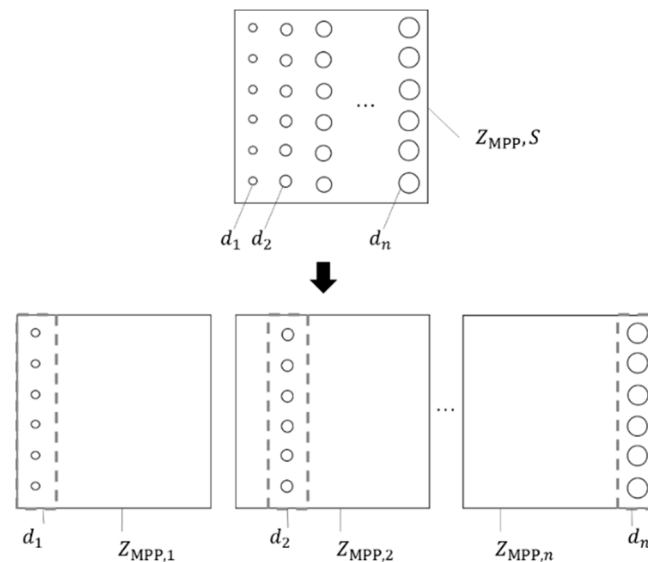

Figure 1. Diagrams of the hypothetical MPPs. The upper MPP is the original MPP, and the lower MPPs are the hypothetical MPPs, which have holes of different diameters only in surface area S.

The surface impedance of the original specimen Z_{MPP} is considered to be the impedance that is obtained when synthesizing the impedances of the hypothetical MPPs, $Z_{MPP,1}$, $Z_{MPP,2}$, $\ldots$, $Z_{MPP,n}$. Therefore, Z_{MPP} is derived by the following equation:

$$Z_{MPP} = \frac{1}{\sum_{i=1}^{n} \frac{1}{Z_{MPP,i}}} \tag{1}$$

where $Z_{MPP,i}$ is the impedance of a hypothetical MPP with holes of diameter d_i. The impedances of the hypothetical MPPs are calculated as follows: a hypothetical impedance $Z_{MPP,i}$ is considered to be the synthesized impedance of the part with the holes and that of the part without holes, which is acoustically rigid. The surface area of the part with holes is S_i, and its impedance is Z_i. The surface area of the part without holes is $(S-S_i)$, and its impedance is Z_{rigid}, which is assumed as infinity. Therefore, $Z_{MPP,i}$ is expressed by the following equation, and this calculation procedure is shown in the diagrams in Figure 2:

$$Z_{MPP,i} = \frac{1}{\frac{1}{Z_i} * \frac{S_i}{S} + \frac{1}{Z_{rigid}} \frac{S-S_i}{S}} = \frac{S}{S_i} Z_i \tag{2}$$

The values of $Z_{MPP,1}$, $Z_{MPP,2}$, $\ldots$, $Z_{MPP,n}$ are calculated using Equation (2) and substituted into Equation (1).

$$Z_{MPP} = \frac{1}{\sum_{i=1}^{n} \frac{S_i}{SZ_i}} = \frac{S}{\sum_{i=1}^{n} \frac{S_i}{Z_i}} = \frac{1}{\sum_{i=1}^{n} r_i Y_i} = \left(\sum_{i=1}^{n} r_i Y_i \right)^{-1} \tag{3}$$
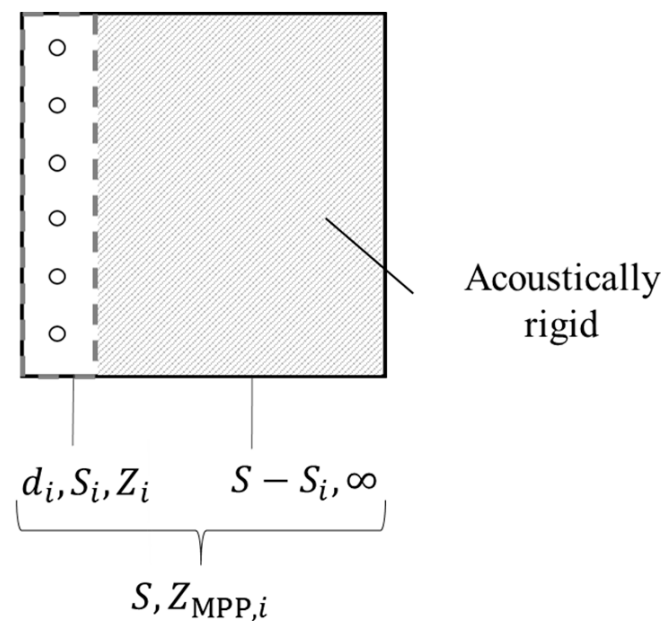
Figure 2. A diagram of the calculation procedure for the impedance of a hypothetical MPP. The area surrounded by the dashed line is the part with holes, and the hatched area is the part without holes, which is acoustically rigid.

By denoting Z_i^{-1} as Y_i, the acoustic admittance, and factor r_i, the equation can be written in the form of the admittance sum method (ASM). In the following calculation, S_i is set to the area occupied by a row of holes, which is determined by the spacing of the holes.

Although the prediction method described above is finally expressed in the form of ASM, the method includes pre-processing by synthesizing the impedances of the hypothetical MPP. Thus, we call this method the synthetic impedance method (SIM) with distinction.

3. Preliminary Study: Applicability of the Synthetic Impedance Method to Various Heterogeneous MPPs

In a previous paper [14], the method presented in the preceding section was validated by four experimental results. Although all the specimens were heterogeneous, they were rather typical in that the combination of the parameters was simple. However, in order to apply the method to more complicated samples, such as dotted-art MPPs, the applicability of the method to a wider variety of parameter distributions needs to be examined.

Therefore, in this section, 12 heterogeneous MPP specimens are used, and their absorption characteristics are measured. Then, the prediction and the measured results are compared to explore the method's predictability.

3.1. Experiment

3.1.1. Specimens

Specimens 1–12 were prepared as heterogeneous MPP specimens. All specimens were made of square aluminum (100 mm sides) with a 0.5 mm thickness, and they were fabricated using precision micro-drilling. The details of each specimen are given below, a photographic summary is given in Figure 3, and a summary of the parameters is given in Table 1.
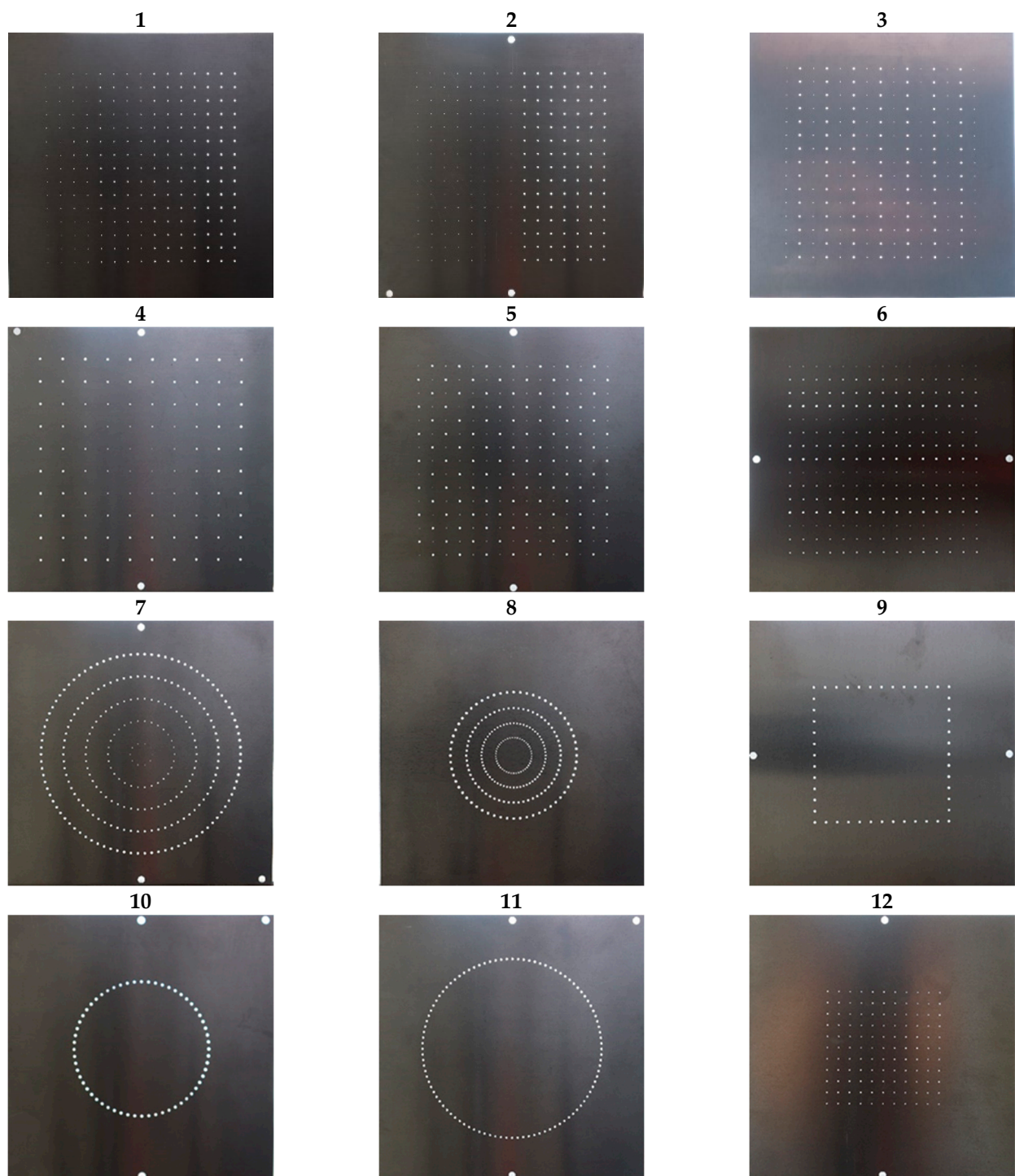
Figure 3. Photographs of specimens1–12.

Table 1. The parameters of specimens 1–12.

Specimen	Diameter (mm) and (Number of Holes)	Hole Separation (mm)	Average Perforation Ratio (%)	Thickness of the Plate (mm)
1	0.3 (60), 0.5 (60), 0.7 (60), 0.9 (45)	6.0	0.6774	0.5
2	0.3 (120), 0.9 (105)	6.0	0.7528	0.5

Table 1. *Cont.*

Specimen	Diameter (mm) and (Number of Holes)	Hole Separation (mm)	Average Perforation Ratio (%)	Thickness of the Plate (mm)
3	0.3 (120), 0.9 (105)	6.0	0.7528	0.5
4	0.3 (4), 0.5 (12), 0.7 (20), 0.9 (28), 1.1 (36)	10.0	0.6236	0.5
5	0.3 (113), 0.9 (112)	6.0	0.7924	0.5
6	0.3 (60), 0.5 (60), 0.7 (60), 0.9 (45)	6.0	0.6774	0.5
7	0.3 (10), 0.5 (30), 0.7 (50), 0.9 (70), 1.1 (90)	3.142 on all circumferences	1.559	0.5
8	0.5 (45), 0.7 (45), 0.9 (45), 1.1 (60)	On all the circumferences from inside to outside: 1.117, 1.518, 2.225, 2.985	1.118	1.0
9	1.0 (48)	5.0	0.3770	0.5
10	1.0 (60)	3.142	0.4712	0.5
11	1.0 (100)	2.513	0.7854	0.5
12	0.5 (121)	5.0	0.2376	0.5

- Specimen 1 consists of four types of holes with diameters of 0.3 mm, 0.5 mm, 0.7 mm, and 0.9 mm, which are arranged in a gradient pattern so that the holes become larger every four rows (due to the limitation of the specimen size, only the 0.9 mm holes are arranged into three rows).
- Specimen 2 consists of two types of holes with diameters of 0.3 mm and 0.9 mm, which are arranged in a solidified manner.
- Specimen 3 consists of two types of holes with diameters of 0.3 mm and 0.9 mm, which are arranged into alternating rows.
- Specimen 4 consists of holes with diameters of 0.3 mm, 0.5 mm, 0.7 mm, 0.9 mm, and 1.1 mm, which are arranged in increasing order from the inner side.
- Specimen 5 consists of two types of holes with diameters of 0.3 mm and 0.9 mm, which are arranged in a checkerboard pattern so that the different holes are adjacent to each other.
- Specimen 6 consists of four types of holes with diameters of 0.3 mm, 0.5 mm, 0.7 mm, and 0.9 mm, arranged into rows of one.
- Specimen 7 consists of five types of holes with diameters of 0.3 mm, 0.5 mm, 0.7 mm, 0.9 mm, and 1.1 mm, which are arranged on circumferences of 10 mm, 30 mm, 50 mm, 70 mm, and 90 mm, respectively, in order from the inside.
- Specimen 8 consists of four types of holes with diameters of 0.5 mm, 0.7 mm, 0.9 mm, and 1.1 mm, which are arranged on circumferences of 16 mm, 29 mm, 42.5 mm, and 57 mm, respectively, in order from the inner side.
- Specimen 9 consists of 1.0 mm diameter holes arranged on a square of 60 mm per side.
- Specimen 10 consists of 1.0 mm diameter holes arranged on a circumference of 60 mm.
- Specimen 11 consists of holes with a diameter of 1.0 mm arranged on a circumference of 80 mm.
- Specimen 12 consists of 0.5 mm diameter holes arranged in the central area of a 50 mm square.

3.1.2. Experimental Setup

The normal incidence absorption coefficient of each sample was measured in accordance with JIS A 1405-2 [25] (ISO 10534-2 compatible [26]) by using a square cross-sectional

impedance tube with a size of 100 by 100 mm. Its maximum measurement frequency was 1700 Hz. The distance between the microphones was 50 mm, and the distance between the specimen surface and the nearest microphone was 100 mm. A photograph of this is shown in Figure 4. The air-back cavity between the specimen and the rigid-back wall was set to four depth conditions, i.e., 25, 50, 75, and 100 mm. A measurement was made at every 1.25 Hz step, from 125 to 1700 Hz.
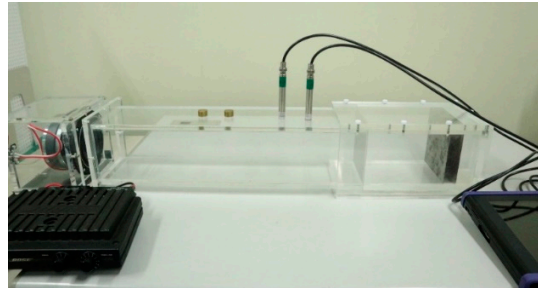

Figure 4. Measurement of the normal incidence absorption coefficient using an impedance tube.

The normal sound absorption coefficients of all specimens were measured using the method described above. Moreover, they were predicted by the synthetic impedance method (SIM) outlined in Section 2 and compared with the measured results. The prediction error indices defined in Section 3.2 were calculated to classify the specimens into groups (1)–(3), as defined in Section 3.2, according to the magnitude of the error.

3.2. Prediction Error Indices and Classification According to the Error

To assess the agreement between the measured and predicted values, numerical error indices were defined; the agreement of the peaks is particularly important, as MPPs exhibit high absorption peaks of certain frequencies. Therefore, three numerical error indices were defined and used later: the relative error of the frequency of the maximum sound absorption, f_{error}; the relative error of the maximum value of sound absorption, i.e., the value of the resonance peak, α_{error}; the *RMS error* of the sound absorption coefficient between 125 and 1700 Hz.

The relative error, f_{error}, of the frequency of the maximum sound absorption coefficient is calculated as follows:

$$f_{error}(\%) = \frac{f_{pre} - f_{mea}}{f_{mea}} \times 100 \tag{4}$$

where f_{pre} is the frequency at which the predicted sound absorption coefficient is maximum, and f_{mea} is that at which the measured sound absorption coefficient is maximum.

The relative error, α_{error}, of the maximum sound absorption coefficient is calculated as follows:

$$\alpha_{error}(\%) = \frac{\alpha_{max,\,pre} - \alpha_{max,mea}}{\alpha_{max,mea}} \times 100 \tag{5}$$

where $\alpha_{max,pre}$ is the maximum value of the predicted sound absorption coefficient, and $\alpha_{max,mea}$ is the maximum value of the measured sound absorption coefficient.

The *RMS error* of the sound absorption coefficient is obtained by the following equation:

$$RMS\ error = \sqrt{\frac{1}{n} \sum_{i=100}^{n} \left(\alpha_{pre,1.25i} - \alpha_{mea,1.25i}\right)^2} \tag{6}$$

where $\alpha_{pre,1\cdot25i}$ is the predicted sound absorption coefficient at $1.25i$ Hz, and $\alpha_{mea,1\cdot25i}$ is the measured sound absorption coefficient at $1.25i$ Hz.

Test specimens 1–12 were classified into groups (1)–(3) according to the magnitude of the error indices. The magnitude of the error index was determined by the average of the absolute values of the four air-back cavity thickness conditions rather than by the value of each air-back cavity condition.

The classification of the specimens into groups were as follows:

- Group (1) has a relative error f_{error} of the frequency with the maximum sound absorption coefficient and a relative error α_{error} of the maximum sound absorption coefficient, both below 5%, and an *RMS* error of 0.05 or less.
- Group (3) has a relative error f_{error} of the frequency of the maximum sound absorption or a relative error α_{error} of the maximum value of sound absorption greater than 10% or an *RMS error* greater than 0.1.
- Specimens that do not fall into either group (1) or (3) were classified into group (2).

The reference values for each abovementioned group were set based on the following considerations: Due to errors in the measurement of the normal incidence absorption coefficient, the measured values of a homogeneous MPP and the values predicted by Guo's theory, which was used in this study, did not completely match. There was an unavoidable error in the measured value—e.g., measurement uncertainty—when it was compared with the value predicted by Guo's theory. Therefore, the sound absorption characteristics of homogeneous MPPs were measured and compared with the predictions made based on Guo's theory to calculate the prediction error, which was then used as the reference value for each indicator. The reference values for each error index were thus determined as described above. Regarding group (2), even if the error indices exceeded this range, a good agreement could still be determined when the graphs were visually examined. Therefore, group (2) comprises a group of specimens for which the present method is applicable, although the error was greater than that of group (1).

Thus, the specimens in groups (1) and (2) were judged to be predictable by the present method, while the specimens in group (3) were judged to be outside the scope of the application of the SIM due to the large and obvious error. To sum up, in this study, f_{error} and α_{error} were both less than 10%, and the *RMS error* was less than 0.1, and these were the reference values used to determine the predictability of the SIM.

3.3. Results and Discussion

Specimens 1–12 were classified into groups (1)–(3), as described above. The results of the classification and the average absolute values of the error indices for the four air-back cavity conditions for each specimen are presented below.

1. Group (1).

This group comprises specimens 1 and 2. As an example, graphs comparing the measured and predicted values for each air-back cavity condition for specimen 1 are shown in Figure 5. The average absolute values of the error indices for the four air-back cavity conditions for each test specimen are shown in Table 2.

Table 2. Mean values of the error indices for the four conditions of air-back cavity depth of specimens 1 and 2.

Specimen	f_{error} (%)	α_{error} (%)	*RMS Error*
1	1.540	3.223	0.04191
2	3.675	2.632	0.03966

2. Group (2).

This group consists of specimens 3, 4, 5, 6, and 7. As an example, graphs comparing the measured and predicted values for each air-back cavity condition of specimen 3 are shown in Figure 6. The average absolute values of the error indices for the four air-back cavity conditions of each test specimen are shown in Table 3.
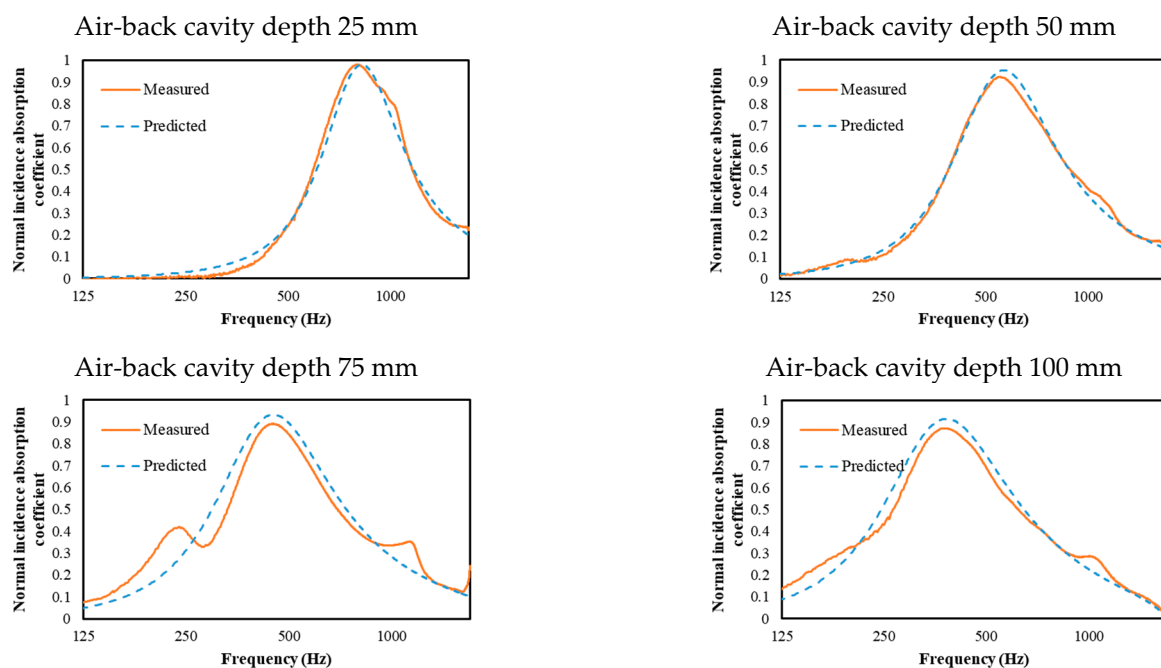
Air-back cavity depth 25 mm

Air-back cavity depth 50 mm

Air-back cavity depth 75 mm

Air-back cavity depth 100 mm

Figure 5. Comparison of the measured and predicted values of the normal incidence sound absorption coefficient of specimen 1. The orange solid line represents the measured values, and the blue dotted line represents the predicted values.

Air-back cavity depth 25 mm

Air-back cavity depth 50 mm

Air-back cavity depth 75 mm

Air-back cavity depth 100 mm

Figure 6. Comparison of the measured and predicted values of the normal incidence sound absorption coefficient of specimen 3. The orange solid line represents the measured values, and the blue dotted line represents the predicted values.
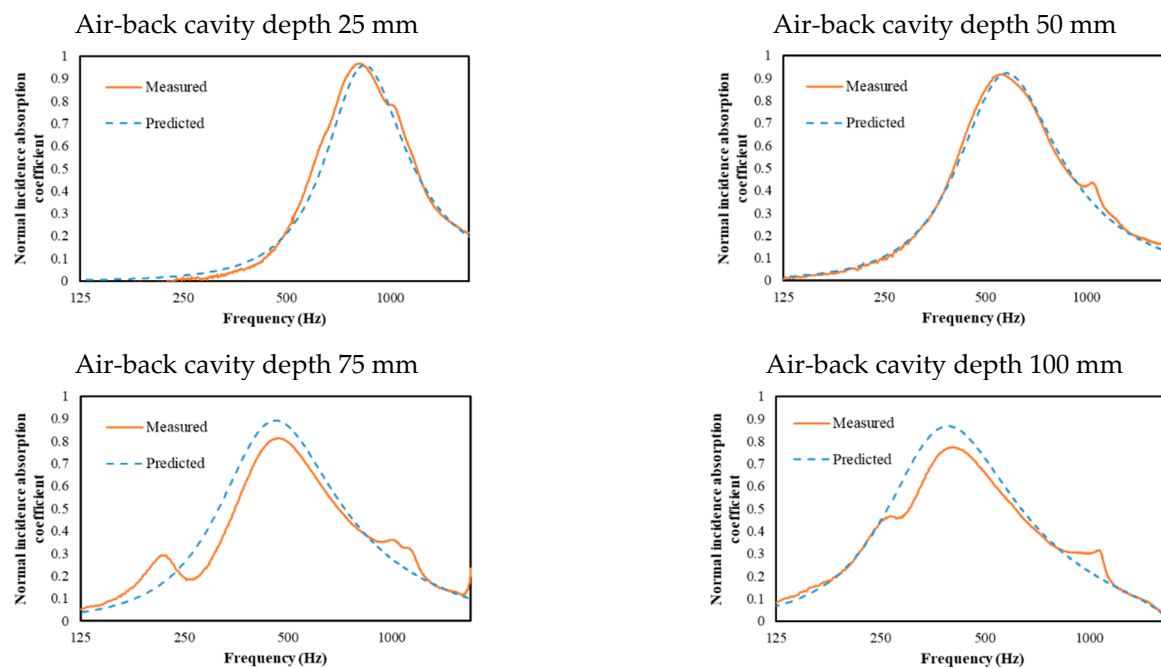
Table 3. Mean values of the error indices for the four conditions of air-back cavity depth of specimens 3, 4, 5, 6, and 7.

Specimen	f_{error} (%)	α_{error} (%)	RMS Error
3	3.591	5.730	0.04853
4	2.704	4.656	0.05104
5	1.038	5.588	0.04313
6	2.242	5.036	0.03980
7	7.938	3.657	0.04662

3.   Group (3).

This group consists of specimens 8, 9, 10, 11, and 12. As an example, graphs comparing the measured and predicted values for each air-back cavity condition of specimen 8 are shown in Figure 7. The average absolute values of the error indices for the four air-back cavity depth conditions of each test specimen are shown in Table 4.
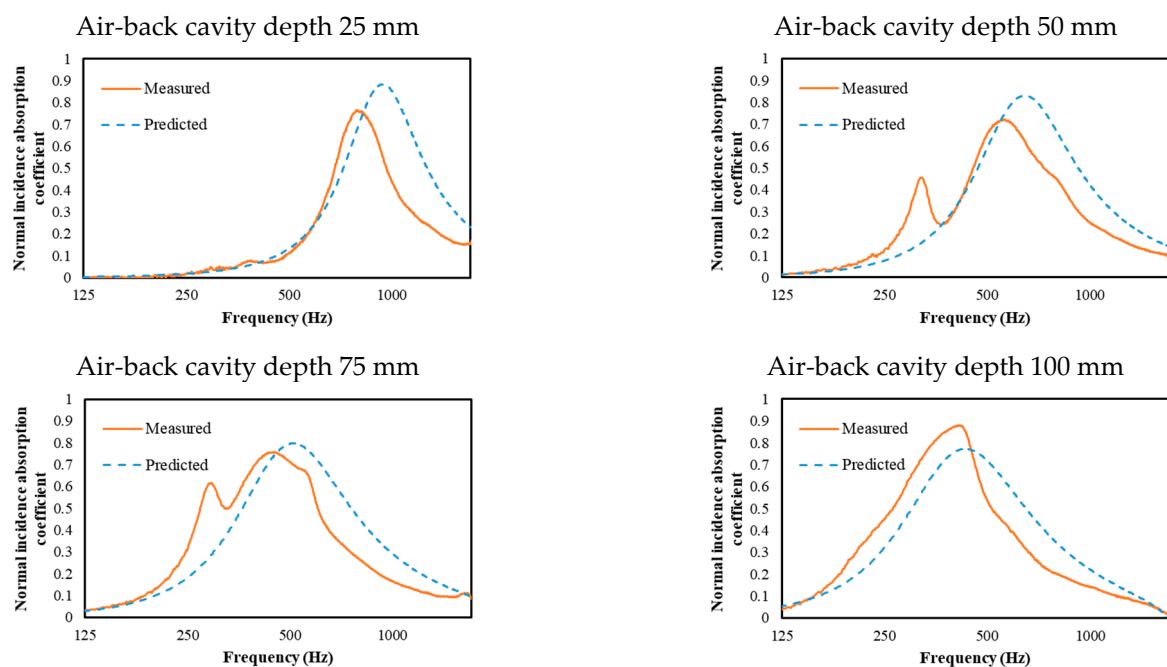

Figure 7. Comparison of the measured and predicted values of the normal incidence sound absorption coefficient of test specimen 8. The orange solid line represents the measured values, and the blue dotted line represents the predicted values.

Table 4. Mean values of the error indices (Equations (4)–(6)) for the four conditions of air-back cavity depth of specimens 8–12.

Specimen	f_{error} (%)	α_{error} (%)	RMS Error
8	13.69	11.95	0.1424
9	4.467	13.39	0.08091
10	2.310	13.24	0.08296
11	9.604	14.29	0.09839
12	11.18	8.632	0.09974

Group (1) is the group whose prediction accuracy is good and the synthetic impedance method (SIM) is judged to be applicable. In all the specimens, the arrangement of the

holes is grid-like, the hole spacing is constant, and the holes are distributed over the entire surface of the specimen.

The common features are as follows:

- The number of hole types with different diameters is between 2 and 4;
- The holes are distributed over the entire surface of the specimen surface;
- The hole spacing is constant.

Group (2) is the group for which the SIM is judged to be applicable; however, the prediction error is larger than that of group (1) but less than the reference value. The arrangement of the holes in specimens 3, 4, 5, and 6 is grid-like, and the hole spacing is constant. The hole spacing of specimen 7 is not constant throughout the specimen. In all test specimens, the holes are distributed over the entire surface.

The common features are as follows:

- The number of different hole types with different diameters is between 2 and 5;
- The holes are distributed over the entire surface of the specimen;
- The hole spacing is not always constant.

Group (3) is the group for which the SIM is considered to not be applicable due to large errors. For all of the specimens, the hole spacing is constant in one part of the specimen surface, but the hole spacing is not constant throughout the entire specimen. In all the specimens, the holes are concentrated and distributed in only one part of the surface.

The common features are as follows:

- The number of hole types with different diameters ranges from 1 to 5;
- The holes are distributed only in some parts of the specimen surface;
- The hole spacing is not constant.

The abovementioned results show that the SIM can be applied to predict the sound absorption characteristics of heterogeneous MPPs that satisfy two conditions common to the specimens in group (1): that the holes are distributed over the entire surface of the specimen, and the hole spacing is constant.

Some of the specimens in group (2), for which the error is acceptable, do not have constant hole spacing. This suggests that the condition of 'constant hole spacing' is not essential, but that it is a condition that enables reliable predictions.

Heterogeneous MPPs with the condition 'holes are distributed only in one part of the specimen surface', which is common to the specimens in group (3), are likely to be outside the scope of the application of the SIM.

With regard to the number of different hole types with different diameters, no specific trend is observed in each group. Therefore, we suggest that the number of hole types with different diameters is unlikely to affect the prediction error.

Regarding the effect of the cavity depth, a comparison of Figures 5–7 shows that there is a tendency for prediction accuracy to become worse in all groups as the air-cavity depth is increased. Carbajo et al. [20] remarks that prediction accuracy for a heterogeneous MPP depends on the cavity configuration, and that the admittance sum method (ASM) is correct in isolated cavity cases. Since the SIM is written in the form of ASM, they are considered to be similar. Therefore, this may be a common feature of ASM and SIM.

4. Investigation by Prototyping Dotted-Art Heterogeneous MPPs

4.1. Design Concept of Dotted-Art Heterogeneous MPPs

In this section, the design of a dotted-art heterogeneous MPP is discussed. Although dotted-art heterogeneous MPPs are design-oriented, it should be possible to predict their absorption coefficient so that they can be effectively used for a target frequency range. Therefore, in this study, a design in which the synthetic impedance method (SIM) can be applied is considered.

From the discussions in the preceding section, the design principle of dotted-art heterogeneous MPPs can be summarized as follows:

- The holes are distributed over the entire surface of the absorber;

- The hole separation is constant over the entire surface of the absorber.

When the two conditions described above are satisfied, heterogeneous MPPs can fall within the scope of the application of the SIM. Therefore, the arrangement of the holes is determined to be grid-like with regular intervals.

With this arrangement, we use two types of holes to illustrate a designed pattern: larger holes and smaller holes. The designed pattern to be illustrated is made with the larger holes, and the background is filled with the smaller holes; in so doing, the pattern made with the larger holes is clearly visible, and the smaller holes in the background are less visible. An example of this concept is shown in Figure 8. In this example, a star-shaped pattern is made with larger holes, and the background is made with smaller holes.
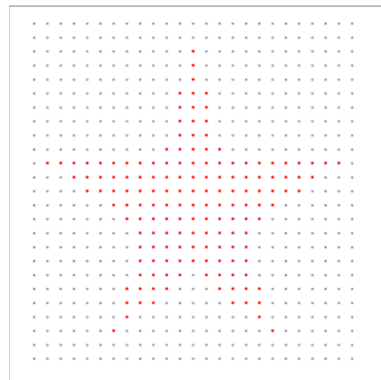

Figure 8. Schematic diagram of the design concept for a dotted-art heterogeneous MPP. In the diagram, the orange dots represent the larger holes of the pattern, and the grey dots represent the smaller holes that comprise the background part.

4.2. Preparation of the Specimens

Based on the design principle described above, nine test specimens are prepared. All specimens are made of aluminum plates (100 mm square) with a 0.5 mm thickness, and they are manufactured using a precision micro-drilling system.

The detailed descriptions of the specimens are as follows (note that, in all specimens, the larger hole size is used for the pattern, and the smaller hole size is used for the background):

- Specimen A is made using 0.2 mm and 0.8 mm diameter holes in a star pattern and with a hole spacing of 4.0 mm.
- Specimen B is made using 0.2 mm and 1.0 mm diameter holes in a star pattern and with a hole spacing of 4.0 mm. The arrangement of the holes is identical to that of specimen A.
- Specimen C is a star pattern with 0.2 mm and 0.8 mm diameter holes, with a hole spacing of 6.0 mm. Although the hole spacing is different, the size of the star is almost the same as that in specimens A and B.
- Specimen D is made with 0.2 mm and 1.0 mm diameter holes and a hole spacing of 6.0 mm to express a star pattern. The arrangement of the holes is identical to that in specimen C.
- Specimen E is made using 0.2 mm and 0.8 mm diameter holes, with a hole spacing of 4.0 mm to produce a star pattern. The hole spacing and the type of holes used are the same as those in specimen A, but the size of the star pattern is smaller than that in specimen E.
- Specimen F is made using 0.2 mm and 0.8 mm diameter holes, with a hole spacing of 4.0 mm and expressing the pattern of a bear face.
- Specimen G is made of 0.2 mm and 0.8 mm holes and a hole spacing of 4.0 mm, which illustrate the bold letters 'KOBE'.
- Specimen H is the outer frame of the bold letters 'KOBE', with holes of 0.2 mm and 0.8 mm in diameter and a hole spacing of 4.0 mm.

- Specimen I is a zigzag pattern, with holes of 0.2 mm and 0.8 mm in diameter and a hole spacing of 4.0 mm.

Photographs of specimens A–I are shown in Figure 9, and the parameters of each specimen are summarized in Table 5.
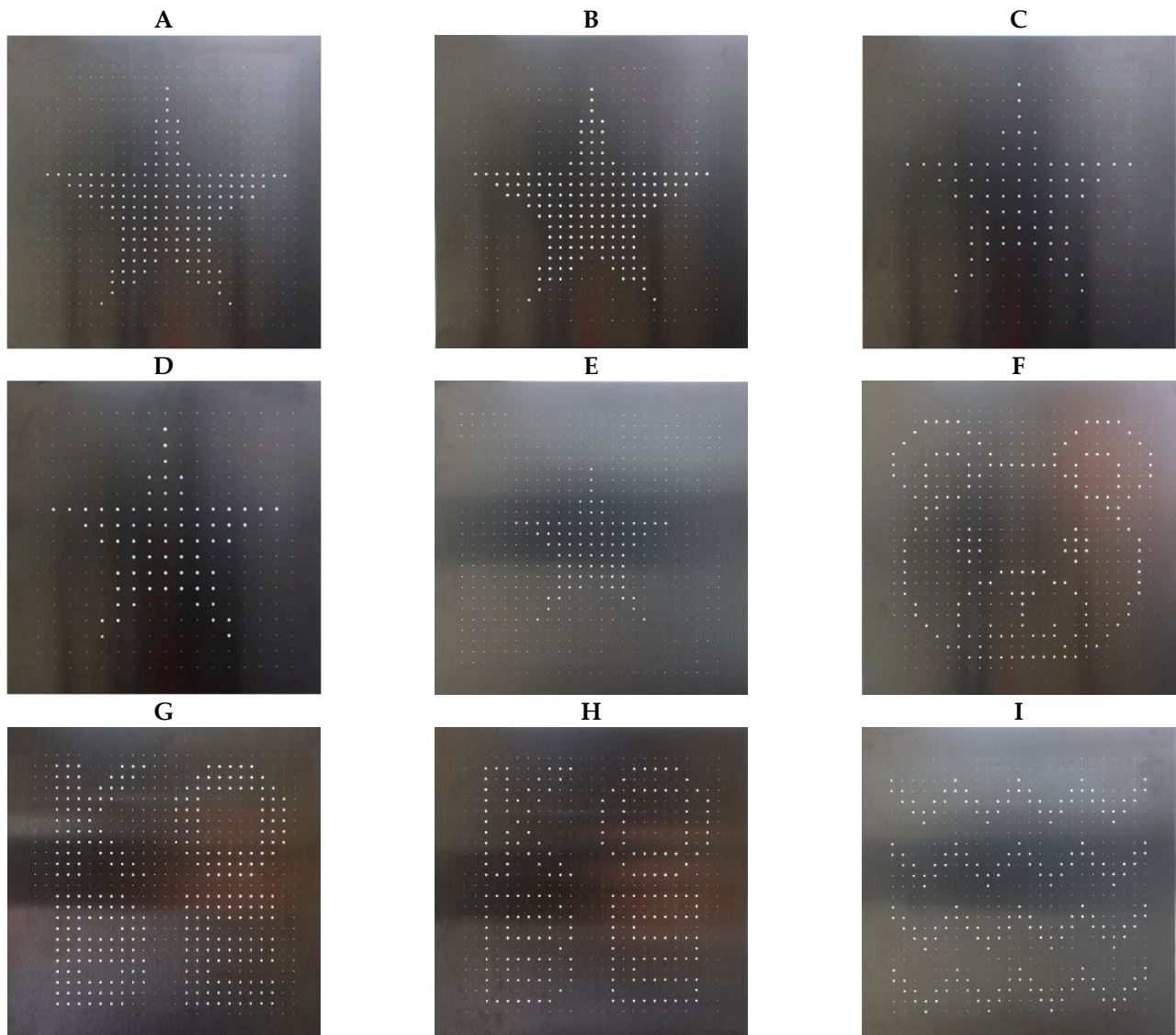
A   **B**   **C**

D   **E**   **F**

G   **H**   **I**

Figure 9. Photographs of specimens A–I.

4.3. Method of Investigating Predictability

The sound absorption characteristics of the dotted-art heterogeneous MPP specimens A–I are measured, and the predicted values are calculated using the SIM described in Section 2. For the prediction error, the error indices from Equations (4)–(6) are used to evaluate the error between these measured and predicted values. The reference values proposed in Section 3.2 are used to determine predictability.

Table 5. Parameters of specimens A–I. Note that the larger hole is used for the pattern, and the smaller hole is used for the background *.

Specimen	Diameter (mm) and (Number of Holes)	Hole Separation (mm)	Average Perforation Ratio (%)	Thickness of the Plate (mm)
A	0.2 (469), 0.8 (156)	4.0	0.9315	0.5
B	0.2 (469), 1.0 (156)	4.0	1.373	0.5
C	0.2 (216), 0.8 (73)	6.0	0.4348	0.5
D	0.2 (216), 1.0 (73)	6.0	0.6412	0.5
E	0.2 (546), 0.8 (79)	4.0	0.5686	0.5
F	0.2 (470), 0.8 (150)	4.0	0.6774	0.5
G	0.2 (318), 0.8 (307)	4.0	1.643	0.5
H	0.2 (417), 0.8 (208)	4.0	1.177	0.5
I	0.2 (425), 0.8 (200)	4.0	1.139	0.5

* In the diameter column, the numbers in parentheses () indicate the number of holes for each diameter.

4.3.1. Experiment

The normal incident sound absorption coefficients of specimens A–I were measured using acoustic tubes. The impedance tube used for the measurements is the same as that in Section 3.1.2. Measurements were made using the transfer function method, in accordance with JIS A1405-2 [25] (ISO 10534-2 [26] compatible), at every 1.25 Hz step up to the upper frequency limit of 1700 Hz. The measurements were carried out under four air-back cavity depth conditions, namely, 25 mm, 50 mm, 75 mm, and 100 mm.

4.3.2. Results and Discussion

In this section, the predictability of the dotted-art heterogeneous MPPs is investigated. In addition, the design of an artistic heterogeneous MPP sound absorber is investigated in terms of prediction accuracy.

The absolute values of the error indices averaged over the four air-back cavity depth conditions for each specimen are shown in Table 6. As an example, graphs comparing the measured and predicted values for specimen A are shown in Figure 10.

Table 6. Mean absolute values of the error indices (Equations (4)–(6)) for the four air-back cavity depth conditions for specimens A–I.

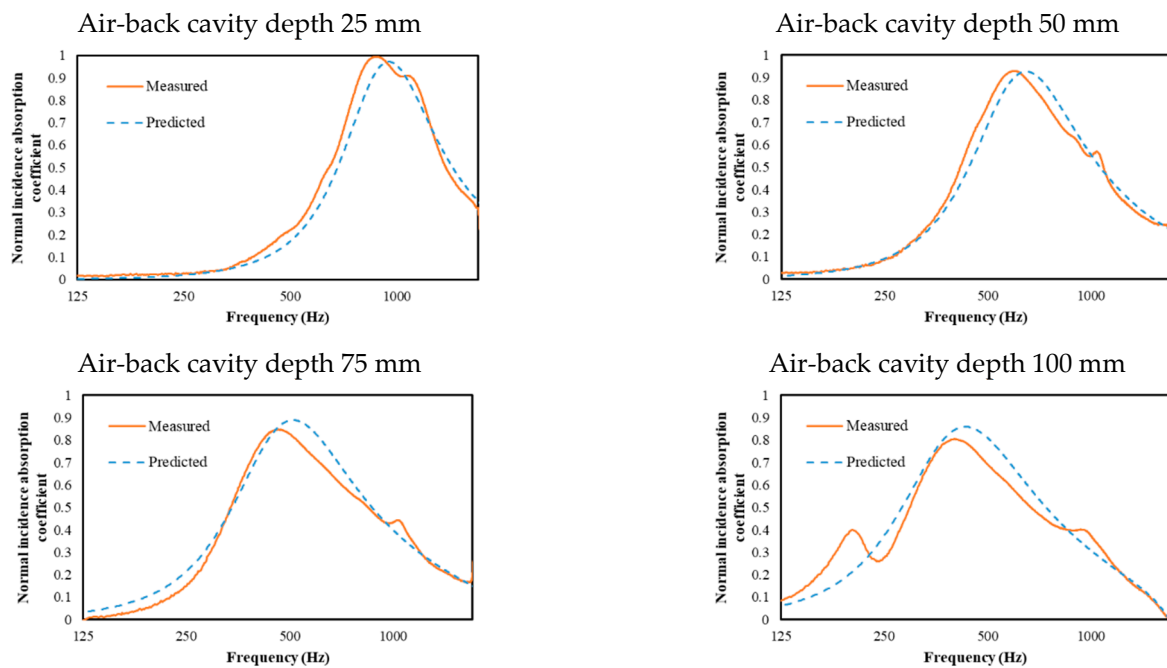| Specimen	f_{error} (%)	α_{error} (%)	*RMS Error*
A	8.598	3.640	0.05230
B	7.356	3.001	0.04935
C	6.846	3.147	0.08007
D	1.100	8.184	0.06381
E	3.205	2.295	0.04886
F	0.8354	5.409	0.03031
G	2.718	4.792	0.03080
H	1.842	4.409	0.02988
I	1.631	2.206	0.02379

Figure 10. Comparison of the measured and predicted values of the normal incidence sound absorption coefficient of test specimen A. The orange solid line represents the measured values, and the blue dotted line represents the predicted values.

Table 6 shows that none of the error indices obtained for the average of the four air-back cavity conditions for specimens A–I exceeded the reference values. This indicates that the sound absorption characteristics of all the dotted-art heterogeneous MPP specimens A–I used in this study can be predicted by the SIM.

4.4. Effect of Hole Distribution on Prediction Accuracy

In this section, the influence of the distribution of the holes on prediction accuracy is studied. For this purpose, numerically evaluating how many holes of the same diameter are unevenly distributed is required, and the degree of this unevenness is used as the criteria in this study. Holes of the same size are considered to be biasedly distributed when the number of each hole found in any part of the surface of the specimen is significantly different from that in the entire specimen.

First, a specimen is divided into smaller parts, $i = 1 \ldots n$. Next, let the proportion of the larger holes to the total number of holes in the entire specimen be taken as the average, x_{av} (%). Then, the proportion of the larger holes x_i (%) to the total number of holes in each part can be calculated to obtain the standard deviation, *SD*.

$$SD = \sqrt{\frac{1}{n} \sum_{i=1}^{n} (x_i - x_{av})^2} \tag{7}$$

The larger the standard deviation, the more biased the distribution of holes is evaluated to be. The arrangement of the holes in specimens A–I is 25 or 17 rows of holes in each direction. In the cases when there are 25 rows of holes in each direction, the specimens are divided into 25 parts, i.e., 5 rows in each direction. In the cases of 17 horizontal rows and 17 vertical rows, it is not possible to divide the specimens into parts of equal size. Therefore, these specimens are divided into four rows in each direction (9 parts), five vertical and four horizontal rows (3 parts), four vertical and five horizontal rows (3 parts), and five horizontal and five vertical rows (1 part); this gives a total of 16 parts. This division is shown schematically in Figure 11. The standard deviation of the proportion of the larger holes to the total number of holes in each section *SD* is calculated for specimens A–I. These

results are shown in Table 7, together with the mean absolute values of the error indices for the four air-back cavity conditions.

(a) **(b)**

Figure 11. Schematic diagram of the division into parts to calculate the standard deviation of the number of the larger holes: (**a**) 25 horizontal and 25 vertical rows; (**b**) 17 horizontal and 17 vertical rows.

Table 7. Comparison of the standard deviation (SD) and error indices (Equations (4)–(6)) of specimens A–I.

Specimen A		Specimen B		Specimen C	
SD	33.45	*SD*	33.45	*SD*	30.72
f_{error} (%)	8.598	f_{error} (%)	7.356	f_{error} (%)	6.846
α_{error} (%)	3.640	α_{error} (%)	3.001	α_{error} (%)	3.147
RMS error	0.05230	*RMS error*	0.04935	*RMS error*	0.08007
Specimen D		Specimen E		Specimen D	
SD	30.72	*SD*	23.96	*SD*	11.81
f_{error} (%)	1.100	f_{error} (%)	3.205	f_{error} (%)	0.8354
α_{error} (%)	8.184	α_{error} (%)	2.295	α_{error} (%)	5.409
RMS error	0.06381	*RMS error*	0.04886	*RMS error*	0.03031
Specimen G		Specimen H		Specimen I	
SD	19.02	*SD*	10.16	*SD*	5.426
f_{error} (%)	2.718	f_{error} (%)	1.842	f_{error} (%)	1.631
α_{error} (%)	4.792	α_{error} (%)	4.409	α_{error} (%)	2.206
RMS error	0.03080	*RMS error*	0.02988	*RMS error*	0.02379

From Table 7, it can be observed that the prediction error tends to be smaller when the standard deviation is small. This suggests that from the point of view of prediction accuracy, it is desirable for the holes to be distributed as unbiasedly as possible in the design of heterogeneous MPPs.

4.5. Effect of the Absence of Holes in the Background on Prediction Accuracy

Not only does the dotted-art heterogeneous MPP proposed in this work require a large number of holes in the patterned part, but it also requires very small holes in the background part, which is time-consuming to produce. Therefore, in this section, we confirm the necessity for small holes in the background part; we also reinforce the idea of creating a dotted-art heterogeneous MPP by combining two types of holes. For this purpose, counterparts without small holes in the background part are produced for specimens A–I; that is, only large holes of the same size are drilled in the patterned part. We name these specimens A′–I′. The average absolute values of the error indices of the measured values of A′–I′ and the predicted values by the SIM for the four conditions of the air-back cavity depth are summarized in Table 8.

Table 8. Mean absolute values of the error indices (Equations (4)–(6)) for the four air-back cavity depth conditions for specimens A–I and A′–I′. 'With' means 'with holes in the background parts', and 'Without' means 'without holes in the background parts'. To compare the 'With' and 'Without' conditions, the smaller values are hatched.

	f_{error} (%)		α_{error} (%)		RMS Error	
	With	**Without**	**With**	**Without**	**With**	**Without**
Specimens A, A′	8.598	9.361	3.640	8.239	0.05230	0.07576
Specimens B, B′	7.356	8.016	3.001	9.256	0.04935	0.08741
Specimens C, C′	6.846	6.413	3.147	8.076	0.08007	0.08845
Specimens D, D′	1.100	1.478	8.184	12.66	0.06381	0.07217
Specimens E, E′	3.205	3.675	2.295	16.06	0.04886	0.1076
Specimens F, F′	0.8354	1.112	5.409	7.030	0.03031	0.05351
Specimens G, G′	2.718	2.236	4.792	5.564	0.03080	0.04364
Specimens H, H′	1.611	4.373	4.640	8.494	0.02988	0.04858
Specimens I, I′	1.631	2.506	2.206	7.442	0.02379	0.03993

In the table, the results for specimens A–I, which also have holes in the background of the pattern, are shown in the 'With' column, while the results for specimens A′–I′, which do not have holes in the background parts, are shown in the 'Without' column, with the smaller values shaded.

The results in Table 8 show that for specimens A′, B′, C′, F′, G′, H′, and I′, none of the error indices exceeds the reference value; i.e., specimens A′, B′, C′, F′, G′, H′, and I′ fall within the applicable range of the SIM. However, for specimens D′ and E′, some of the error indices exceed the reference value and are outside the applicable range of the SIM, whereas specimens D and E are within the applicable range of the SIM. It was then concluded that for the dotted-art heterogeneous MPPs, the ones without the smaller holes in the background part may be out of the scope of application of the SIM.

A comparison of each specimen with and without holes in the background part is discussed. For specimens A, B, D, E, F, H, and I, all three error indices were found to be smaller than those for specimens A′, B′, D′, E′, F′, H′, and I′, respectively. The relative errors for the frequencies of maximum sound absorption were smaller for specimens C′ and G′ without holes in the corresponding backgrounds, but for the other two error indices, they were smaller than those for specimens C′ and G′. This indicates that the dotted-art heterogeneous MPP with a combination of two types of holes with different diameters tends to have better prediction accuracy than the specimen without holes in the background parts.

These results show that the SIM can also be applied to dotted-art heterogeneous MPPs with only one type of hole in the patterned part. Dotted-art MPPs without smaller holes filling the background part are similar to the prototypes used by Lee et al. [11]. In such a case, if the manufacturing accuracy is better and the estimation of the area of the perforated part is adequate, it may be possible to obtain a reasonable prediction accuracy with the SIM. However, a design combining two types of holes is more appropriate in terms of prediction error.

5. Conclusions

This work aimed to propose a design concept for a dotted-art-designed heterogeneous MPP, whose sound absorption characteristics could theoretically be predicted by the method proposed by the authors, which was called the synthetic impedance method (SIM) in a previous work [20].

First, the SIM for the prediction of the absorption characteristics of a heterogeneous MPP was summarized. In this study, considering that the SIM was applied to predict the absorption characteristics of dotted-art heterogeneous MPPs, the scope of its application was examined. Twelve specimens of heterogeneous MPPs were produced, and their normal incidence absorption coefficients were measured. The measured results were compared

with the theoretically calculated results by the presented method. Close investigations were performed using the proposed error indices, i.e., f_{error}, α_{error}, and *RMS error*. From the investigations, the following were found:

- The SIM can predict the sound absorption characteristics of heterogeneous MPPs that satisfy the following two conditions: (1) the holes are distributed over the entire surface of the specimen, and (2) the hole spacing is constant.
- The condition of constant hole spacing is not essential for the application of the SIM, but it is considered to be a condition that enables a more reliable prediction.
- Heterogeneous MPPs with holes that are distributed in only a limited part of the specimen surface are likely to be outside the scope of the application of the SIM.
- When using the SIM to predict the sound absorption properties of heterogeneous MPPs, a number of different hole sizes is unlikely to influence prediction accuracy.

Next, considering the findings described above, a concept for the design of a dotted-art heterogeneous MPP was proposed. Knowing that holes should be distributed over the entire surface of the absorber, the proposed concept makes use of two types of holes, i.e., larger holes to illustrate the patterned part and smaller holes to fill the background. The holes were arranged in a grid with regular intervals over the entire surface to satisfy the conditions for heterogeneous MPPs to which the SIM could be applied.

According to this concept, nine specimens were prepared. The predictability of each specimen by the SIM was examined with the error indices proposed above. By doing this, the design concept was discussed in terms of prediction errors. The findings of the study are described below.

- The prediction accuracy for the specimens of dotted-art heterogeneous MPPs, designed according to the concept described above, tends to be good. This is because holes of the same diameter are unbiasedly distributed over the surface; i.e., the distribution of holes of the same diameter is less biased. Therefore, for the design of a dotted-art heterogeneous MPP, the distribution of holes of the same diameter should be as unbiased as possible.
- For dotted-art heterogeneous MPPs with a combination of two types of holes with different diameters: If the smaller holes in the background area are removed and only one type of hole is used in the patterned area of the heterogeneous MPP, the SIM is still applicable to the specimens (without smaller holes); however, prediction accuracy decreases. Therefore, a dotted-art heterogeneous MPP with two types of holes is better in terms of prediction accuracy.

Appendix A. Outline of Guo's Theory

Guo's model [21] was employed to calculate the acoustic impedance of MPPs throughout this work. It is summarized by Bolton and Kim [22], Herdtle et al. [23], Okuzono et al. [24], etc. In this appendix, only an outline of the theory is given for the readers' convenience.

Let the impedance of MPP be Z_t, which is expressed as

$$Z_t = \frac{j\omega\rho_e t}{\varepsilon} + \frac{\alpha 2 R_s}{\varepsilon} + \frac{j\omega\rho_0\delta}{\varepsilon} \tag{A1}$$

where ω, t, ε, and δ are the angular frequency (rad/s), panel thickness (m), perforation ratio (-), and end correction factor, respectively.

The first term of Equation (A1) indicates the effect of the viscous energy loss inside the hole: here ρ_e is the effective density, which is expressed by the following equation in the case of a circular hole:

$$\rho_e = \rho_0 / \left[1 - \frac{2}{s\sqrt{-j}} \frac{J_1(s\sqrt{-j})}{J_0(s\sqrt{-j})} \right], \tag{A2}$$

where J_0 and J_1 are the zeroth- and first-order Bessel functions of the first kind, respectively. The parameter s in Equation (A2) in the case of a circular hole is defined as follows:

$$s = r\sqrt{\omega\rho_0/\eta}, \tag{A3}$$

where r is the radius (m), and η is the viscosity of the air (kg/m/s). In the case of the micro-perforation of an arbitrary cross-sectional shape, ρ_e is given as follows:

$$\rho_e = \rho_0 \left(1 + \frac{\sigma\varphi}{j\omega\rho_0} G_c(s) \right) \tag{A4}$$

where $\sigma\phi$ is the flow resistivity (Pa s/m^2); this becomes $\sigma\phi = 8\eta/r_p^2$ in the case of a square hole, with r_p as the parameter defined by the perimeter of the cell l (m) and the cross-sectional area S (m^2), which is the equivalent radius $r_p = 2S/l$ (m). $G_c(s)$ is given as follows:

$$G_c(s) = -\frac{s}{4}\sqrt{-j}\frac{J_1(s\sqrt{-j})}{J_0(s\sqrt{-j})} / \left[1 - \frac{2}{s\sqrt{-j}} \frac{J_1(s\sqrt{-j})}{J_0(s\sqrt{-j})} \right] \tag{A5}$$

with

$$s = c\sqrt{8\omega\rho_0/\sigma\phi} \tag{A6}$$

The second term in Equation (A1) indicates the end correction due to surface admittance, and parameter R_s is given by the following equation:

$$R_s = \sqrt{2\eta\rho_0\omega}/2 \tag{A7}$$

The coefficient α in the second term of Equation (A1) is dependent on the shape of the edge of the perforation. This means that Guo's theory depends on the sharpness of the edge: When the cross-section of the hole edge is rounded, it is 2.0; if it is sharp, the value is 4.0. The third term is the end correction, expressed by δ for a circular hole, $\delta = \delta_c$, as follows:

$$\delta_c = 0.85d \left(1 - 1.13\varepsilon^{1/2} - 0.09\varepsilon + 0.27\varepsilon^{3/2} \right) \tag{A8}$$

References

1. Maa, D.-Y. Theory and design of microperforated panel sound-absorbing constructions. *Sci. Sin.* **1975**, *17*, 55–71.
2. Sakagami, K.; Okuzono, T. Some considerations on the use of space sound absorbers with next-generation materials reflecting COVID situations in Japan: Additional sound absorption for post-pandemic challenges in indoor acoustic environments. *UCL Open Environ.* **2020**, *1*, 9. [CrossRef]
3. Kang, J.; Fichs, H.V. Predicting absorption of open weave textiles and micro-perforated membranes backed by an air space. *J. Sound Vib.* **1999**, *220*, 905–920. [CrossRef]
4. Fuchs, H.V.; Zha, X.; Zhou, X.; Drotleff, H. Creating low-noise environments in communication rooms. *Appl. Acoust.* **2001**, *62*, 1375–1396. [CrossRef]

5. Zha, X.; Fuchs, H.V.; Drotleff, H. Improving the acoustic working conditions for musicians in small spaces. *Appl. Acoust.* **2002**, *63*, 203–221. [CrossRef]

6. Kang, J.; Brocklesby, M.W. Feasibility of applying micro-perforated absorbers in acoustic window systems. *Appl. Acoust.* **2005**, *66*, 669–689. [CrossRef]

7. Asdrubali, F.; Pispola, G. Properties of transparent sound-absorbing panels for use in noise barriers. *J. Acoust. Soc. Am.* **2007**, *121*, 214–221. [CrossRef]

8. Herrin, D.; Liu, J.; Seybert, A. Properties and applications of microperforated panel. *Sound Vib.* **2011**, *45*, 6–9.

9. Herrin, D. A guide to the applications of microperforated panel absorbers. *Sound Vib.* **2017**, *51*, 12–18.

10. Adams, T. *Sound Materials: A Compendium of Sound Absorbing Materials for Architecture and Design*; Frame Pub: Amsterdam, The Netherland, 2017; pp. 214–231.

11. Lee, H.P.; Kumar, S.; Aow, J.W. Proof-of-concept design for MPP acoustic absorbers with element of art. *Designs* **2021**, *5*, 72. [CrossRef]

12. Maa, D.-Y. Microperforated-panel wideband absorbers. *Noise Control Eng. J.* **1987**, *29*, 77–84. [CrossRef]

13. Maa, D.-Y. Potential of microperforated panel absorber. *J. Acoust. Soc. Am.* **1998**, *104*, 2861–2866. [CrossRef]

14. Kusaka, M.; Sakagami, K.; Okuzono, T. A basic study on the absorption properties and their prediction of heterogeneous micro-perforated panels; A case study of micro-perforated poanels with heterogeneous hole size and perforation ratio. *Acoustics* **2021**, *3*, 473–484. [CrossRef]

15. Sakagami, K.; Nagayama, Y.; Morimoto, M.; Yairi, M. Pilot study on wideband sound absorber obtained by combination of two different microperforated panel (MPP) absorbers. *Acoust. Sci. Technol.* **2009**, *30*, 154–156. [CrossRef]

16. Yairi, M.; Sakagami, K.; Takebayashi, K.; Morimoto, M. Excess sound absorption at normal incidence by two microperforated panel absorbers with different impedance. *Acoust. Sci. Technol.* **2011**, *32*, 194–200. [CrossRef]

17. Mosa, A.I.; Putra, A.; Ramlan, R.; Esraa, A. Wideband sound absorption of a double-layer microperforated panel with inhomogeneous perforation. *Appl. Acoust.* **2020**, *161*, 107167. [CrossRef]

18. Pan, L.; Martellotta, F. A parametric study of the acoustic performance of resonant absorbers made of micro-perforated membranes and perforated panels. *Appl. Sci.* **2020**, *10*, 1581. [CrossRef]

19. Sakagami, K.; Kusaka, M.; Okuzono, T.; Nakanishi, S. The effect of deviation due to the manufacturing accuracy in the parameters of an MPP on its acoustic properties; Trial production of MPPs of different hole shapes using 3D printing. *Acoustics* **2020**, *2*, 605–616. [CrossRef]

20. Carbajo, J.; Ramis, I.; Godinho, L.; Amado-Mendes, P. Assessment of methods to study the acoustic properties of heterogeneous perforated panel absorbers. *Appl. Acoust.* **2018**, *133*, 1–7. [CrossRef]

21. Guo, Y.; Allam, S.; Abon, M. Micro-Perforated Plates for Vehicle Applications. In Proceedings of the Inter-Noise 2008, Shanghai, China, 26–29 October 2008.

22. Bolton, J.S.; Kim, N. Use of CFD to calculate the dynamic resistive end correction for microperforated materials with tapered holes. *Acoust. Aust.* **2010**, *38*, 134–144.

23. Herdtle, T.; Bolton, J.S.; Kim, N.; Alexander, J.H.; Gardes, R.W. Transfer impedance of microperforated materials with tapered holes. *J. Acoust. Soc. Am.* **2013**, *134*, 4752–4762. [CrossRef] [PubMed]

24. Okuzono, T.; Nitta, T.; Sakagami, K. Note on microperforated panel model using equivalent-fluid-based absorption elements. *Acoust. Sci. Technol.* **2019**, *40*, 221–224. [CrossRef]

25. *JIS A 1405-2: 2007*; Acoustics—Determination of Sound Absorption Coefficient and Impedance in Impedance Tubes—Part 2: Transfer-Function Method. JIS: Tokyo, Japan, 2007.

26. *ISO 10534-2:1998*; Acoustics—Determination of Sound Absorption Coefficient and Impedance in Impedance Tubes—Part 2: Transfer-Function Method. ISO: Geneva, Switzerland, 1998.